Plasmonics (2013) 8:63–70
DOI 10.1007/s11468-012-9422-9

SiC Multilayer Structures as Light Controlled Photonic Active Filters

M. A. Vieira · M. Vieira · P. Louro · V. Silva · J. Costa · A. Fantoni

Received: 8 May 2012 / Accepted: 6 August 2012 / Published online: 17 August 2012

Abstract Tunable wavelength division multiplexing converters based on amorphous SiC multilayer photonic active filters are analyzed. The configuration includes two stacked p-i-n structures (p(a-SiC:H)-i'(a-SiC:H)-n(a-SiC:H)-p(a-SiC:H)-i(a-Si:H)-n(a-Si:H)) sandwiched between two transparent contacts. The manipulation of the magnitude is achieved through appropriated front and back backgrounds. Transfer function characteristics are studied both theoretically and experimentally. An algorithm to decode the multiplex signal is established. An optoelectronic model supports the optoelectronic logic architecture. Results show that the light-activated device combines the demultiplexing operation with the simultaneous photodetection and self-amplification of an optical signal. The output waveform presents a nonlinear amplitude-dependent response to the wavelengths of the input channels. Depending on the wavelength of the external background and irradiation side, it acts either as a short- or a long-pass band filter or as a band-stop filter. A two-stage active circuit is presented and gives insight into the physics of the device.

Keywords Optical sensors · Optical filters · Numerical and electrical simulations · Optoelectronic model

M. A. Vieira (✉) · M. Vieira · P. Louro · V. Silva · J. Costa · A. Fantoni
Electronics Telecommunication and Computer Department, ISEL,
R. Conselheiro Emídio Navarro,
1949-014 Lisbon, Portugal
e-mail: mv@isel.ipl.pt

M. A. Vieira · M. Vieira · P. Louro · V. Silva · J. Costa · A. Fantoni
CTS-UNINOVA,
Quinta da Torre, Monte da Caparica,
2829-516 Caparica, Portugal

M. Vieira
DEE-FCT-UNL,
Quinta da Torre, Monte da Caparica,
2829-516 Caparica, Portugal

Introduction

Systems that transmit, receive, and/or process intelligence require some sort of modulation, which is the deliberate distortion of a carrier to impress intelligence (data) upon it and subsequently allows information recovery. Data transmission can be improved using the wavelength division multiplexing–demultiplexing technique, WDM [1]. Multilayered Si/C structures based on amorphous silicon technology are expected to become reconfigurable to perform WDM optoelectronic logic functions [2, 3]. Filters are used to emphasize signals in a certain wavelength range and to reject signals in other ranges. They have a nonlinear magnitude-dependent response to each incident light wave. This nonlinearity provides the possibility for selectively removing and adding a specific wavelength and can be used to boost signal after multiplexing or before demultiplexing.

Double pi'n/pin a-SiC:H heterostructures, through an adequate engineering design of the multiple layers' thickness, absorption coefficient, and dark conductivities, can accomplish those functions [4, 5]. Here, we propose a photodetector with integrated optical thin film filters. By means of optical bias control applied to the device, the photonic function may be modified, giving reconfiguration. A new method is presented for optical routing using wavelength background processing techniques

Device Optimization

Operation and Design

In the WDM signal transmission, different pulsed channels (color channels) are transmitted together and demultiplexed using, usually, a photodetector and different external wavelength selective filters. Here, by superimposing background

illumination with different wavelengths to the pulsed channel the WDM device behaves itself as an integrated active filter, producing signal attenuation or, as an amplifier, producing signal gain, depending on the channel/background wavelength combination. This effect avoids the use of external filters and is reported and fully discussed elsewhere [6].

The wavelength selective photodetector is a multilayered heterostructure based on a-Si:H and a-SiC:H materials produced by PE-CVD at 13.56 MHz radio frequency. The configuration of the device, shown in Fig. 1, includes two stacked p-i-n structures (p(a-SiC:H)- i'(a-SiC:H)-n(a-SiC:H)-p(a-SiC:H)-i(a-Si:H)-n(a-Si:H)) sandwiched between two transparent contacts (ITO). Low conductivity doped layers were used to enhance the light-to-dark conductivity of the device, carbon was added during the deposition process to tailor the absorption coefficients across the active intrinsic layers. So, the thicknesses and optical gap of the i'- (200 nm; 2.1 eV) and i- (1,000 nm; 1.8 eV) layers are optimized for light absorption in the blue and red ranges, respectively [7]. As a result, both front and back pin structures act simultaneously as optical filters confining, respectively, the blue photogenerated carriers at the front diode (pin_1) and the red ones at the back diode (pin_2).

The device operates within the visible range using as input color channels (data) a wave-modulated light (external regulation of frequency and intensity) square supplied by a red (λ_R=624 nm), a green (λ_G=526 nm), and a blue (λ_B=470 nm) LED. Steady-state optical bias with different wavelength and intensities (background) was superimposed from the front (pin_1) and back (pin_2) sides and the photocurrent measured at −8 V. As background wavelengths, violet (λ_{Vback}=400 nm), red (λ_{Rback}=624 nm), green (λ_{Gback}=524 nm), and blue (λ_{Bback}=470 nm) illumination were used.

Light Confinement

To better understand the light filtering properties of the device, we used a device simulation program ASCA-2D to analyze the spectral sensitivity in the device. The generation rate is calculated following a Urbach–Tauc–Lorentz model [8] for the absorption coefficients. The input parameters were obtained based on the experimental results of the front and back diodes [4].

In Fig. 2, the simulated spectral sensitivity of the front (pin_1) and back (pin_2) diodes (lines) are compared with the normalized experimental sensitivity of the individual front and back diodes (symbols). A good fit between simulated and experimental results was achieved for the individual optimized diodes. As a result, both front and back pin structures act separately as optical filters confining, respectively, the blue and the red optical carriers to their active absorption areas.

Based on the optimized input parameters for the absorption coefficients, Fig. 3 reports the simulated generation/recombination rate profiles across whole device, under front and back violet optical bias. Results show that the depth of light penetration within the device depends on both the wavelength of the input channels and background. If the light in the background is a short wavelength radiation (violet), the photogeneration profile is strongly influenced by the choice of the device side for light incidence. When compared with the absence of background light, under front irradiation, the generation in the front diode increases mainly for the long wavelengths channels (green and red) due to the contribution of the background light that generates carriers exclusively in the front diode. Under back irradiation, the generation in the back photodiode increases for short/medium wavelengths due to the light penetration depth of the violet light across the bottom of the a-Si:H intrinsic layer.

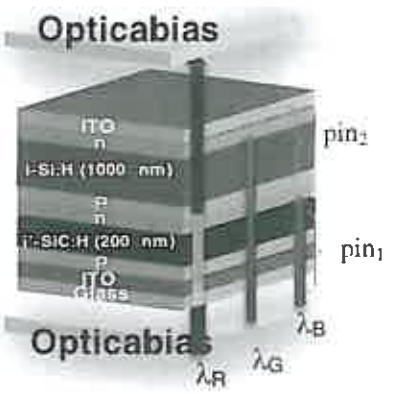

Fig. 1 Device design and operation

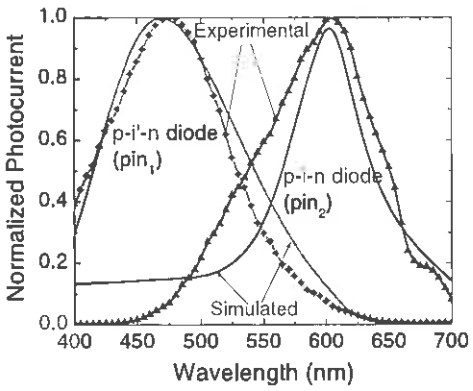

Fig. 2 Comparison between simulated (*lines*) and experimental (*symbols*) normalized front (p-i'-n) and back (p-i-n) diodes

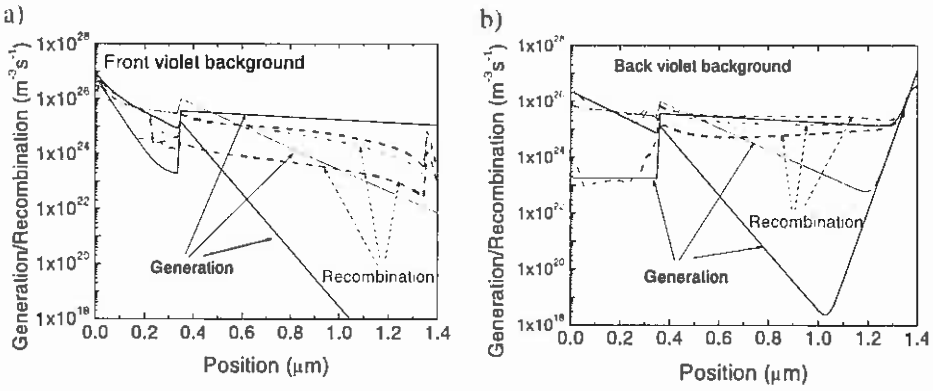

Fig. 3 Generation/recombination rate profiles of the device under: **a** front and **b** back steady-state violet illumination

Spectral Sensitivity

Influence of the Background Intensity

In Fig. 4, at 2,000 Hz, the spectral photocurrent under different background intensities is displayed under red (a), green (b), blue (c), and violet (d) backgrounds and without it. The steady-state optical bias was applied from the front (pin_1, solid symbols) and back (pin_2, open symbols) sides. The values were normalized to the maximum value without background.

Results show that the sensitivity is much higher under front than under back irradiation. Under front violet or blue, when compared with the response without optical bias (see arrows in figures), the sensitivity increases with the decrease of the background wavelength and increases with its intensity. Under red irradiation, an opposite behavior is detected. So, under low wavelength backgrounds (violet or blue), the device acts as a long-pass filter for wavelengths higher than 500 nm and as an active short-pass filter for this wavelength, under red irradiation. Under front green background, the device is a band-rejection filter that works to screen out

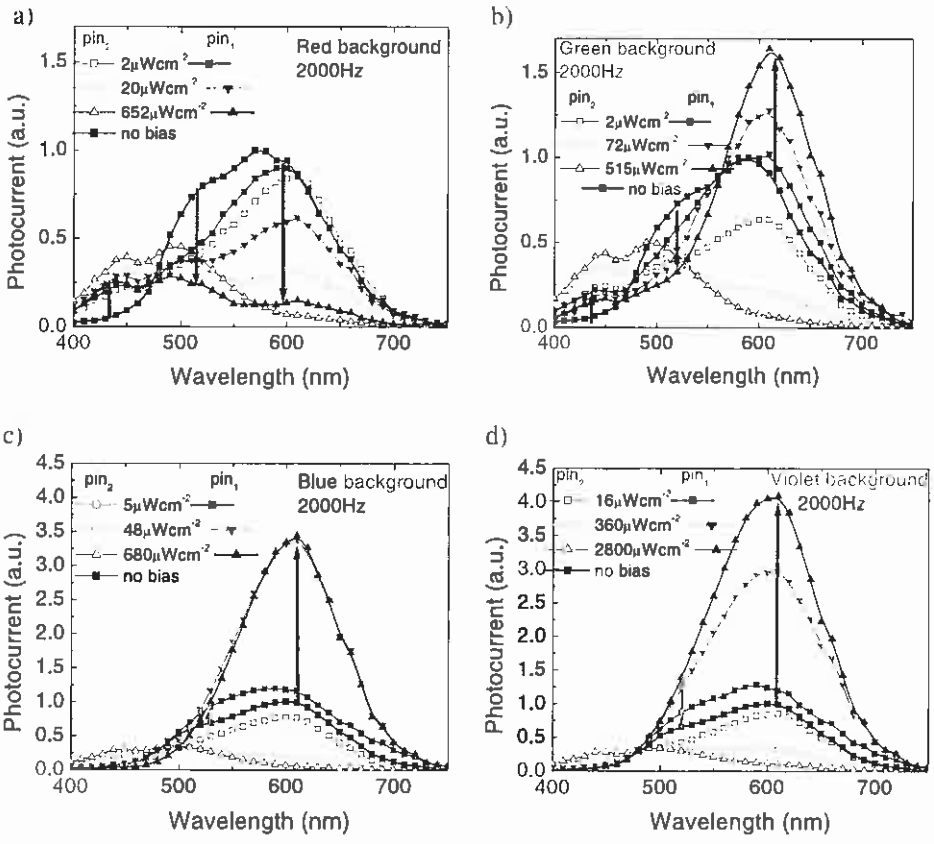

Fig. 4 Spectral photocurrent without and under different background intensities and wavelengths: red (**a**), green (**b**), blue (**c**), and violet (**d**) backgrounds. The optical bias is applied from the front (*solid symbols*) and from the back (*open symbols*) sides

wavelengths that are within the medium range (475–550 nm), giving easy passage at all wavelengths below and above. The back irradiation, whatever the background wavelength, strongly quenches the sensitivity in the long wavelengths (>550 nm) and enhances it at the short wavelengths acting as a short-pass filter with a gain that increases with the intensity.

Influence of the Irradiation Side

In Fig. 5, the spectral photocurrent, normalized to its value without background is displayed, under front (a) and back (b) violet irradiations and different intensities. A peak fit adjustment to the data was performed (lines) with peaks centered on 630 nm (solid), 520 nm (dash), and 430 nm (dot).

Results show that under violet irradiation, as the background intensity increases, the peak centered at 630 nm (red range) strongly increases, while under back light, an opposite behavior is observed and the red peak is strongly reduced (see arrows). Under front and back side irradiation, the peak at 520 nm (green range) increases slightly with the intensity. Under back irradiation, a new peak centered at 430 nm appears and increases with the background intensity. So, under front illumination, the reddish part of the spectrum is strongly enhanced with the intensity, while under back illumination the main enhancement occurs at the blue region. So, under short wavelength irradiation and appropriated intensity, by changing the irradiation side, the front and the back diodes can be tuned separately.

Photonic Active Filters

Input Signals

To analyze the device under information-modulated wave and uniform irradiation, three monochromatic pulsed lights separately (red, green, and blue input channels) or their combination (MUX signal) illuminated the device. Steady-state red (652 $\mu W cm^{-2}$), green (515 $\mu W cm^{-2}$), blue (680 $\mu W cm^{-2}$), and violet (2,800 $\mu W cm^{-2}$) optical bias was superimposed separately from the front (pin_1) and the back (pin_2) sides and the photocurrent measured at −8 V.

In Fig. 6, the transient results for the input channels are displayed. In Table 1, the gains (α), defined as the ratio between photocurrents under irradiation and without it, for the red, green, and blue input channels are presented. Here, the superscripts are related to the background wavelength (R, G, B, and V) and the subscripts ($R,pin_{1,2}$, $G,pin_{1,2}$, and $B,pin_{1,2}$) to the channel color and irradiation side.

The results show that, even under transient conditions, the effect of the background wavelength and impinging side presents the same nonlinear dependence as in Fig. 4. Violet and blue radiations are absorbed at the top or across the front diode (pin_1), increasing the electric field at the least absorbing cell [7], the back diode (pin_2), where the red and part of the green channels generate the carriers. So, the red and the green channel collections are enhanced while the blue one stays near its dark value or slightly decreases. Red irradiation has an opposite effect, increases the electric field at the front diode, and quenches it in the back one amplifying the blue channel response. Under green steady-state background, the electric field is balanced between both front and back diodes and the collection depends mainly on the channel wavelength.

Results have shown that the morphology of filter results from the interaction of the electric field under applied optical bias (red, green, blue, and violet) and the transient electric field induced by the input channels (red, green, and blue). This interaction results in electric field lines that guide the photocarriers generated by the input channels.

In Fig. 7, the simulated electric field profile, under back violet background without channels (OFF) or with the red, green, and blue channels ON (ON) are displayed. Results show that the flow rate of the carriers through those field

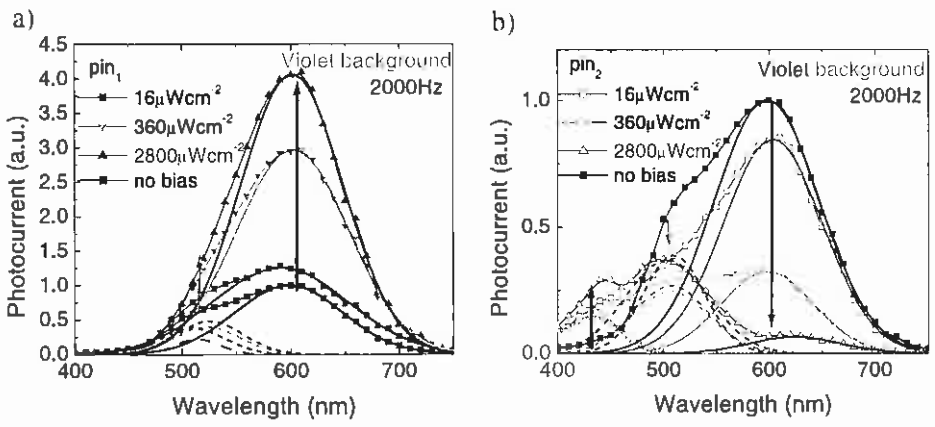

Fig. 5 Normalized spectral photocurrent under front (a) and back (b) violet irradiations with different intensities

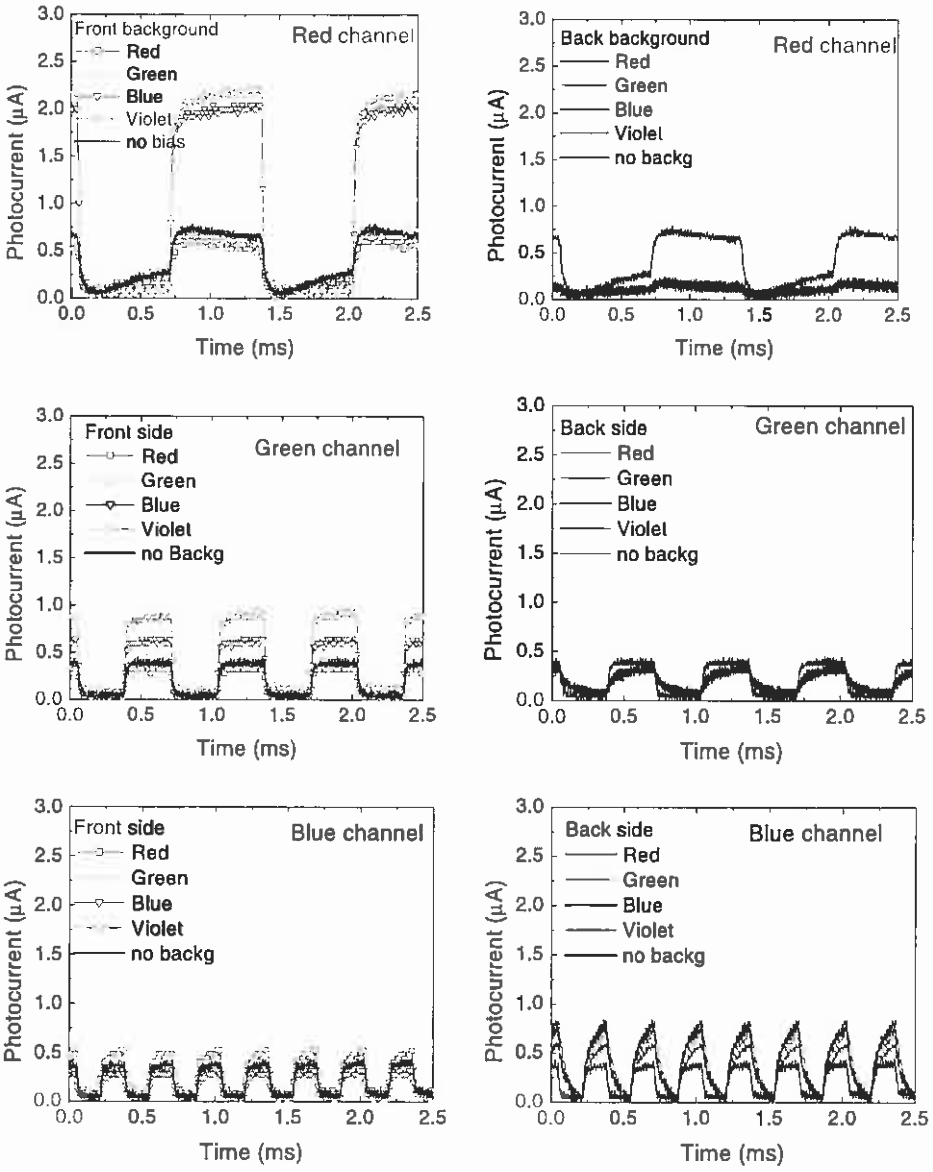

Fig. 6 Input red, green and blue transient signals at −8 V without (no bias) and with: red (R), green (G), blue (B), and violet (V) optical bias from the front (pin_1—*left*) and back (pin_2—*right*) sides

lines towards the output depends on the *on/off* state of the channels. Under back irradiation, the small absorption depth of the violet photons across the back diode (Fig. 3) quenches

Table 1 Gains ($\alpha^{R,\ G,B,V}{}_{R,G,B\ pin1,2}$) at the input red, green, and blue channels wavelengths

Channels	α^R	α^G	α^B	α^V
$\alpha_{R,pin1}$	0.83	1.01	2.84	3.09
$\alpha_{R,pin2}$	0.14	0.19	0.19	0.19
$\alpha_{G,pin1}$	0.92	1.03	1.64	2.21
$\alpha_{G,pin2}$	0.79	0.77	0.82	0.74
$\alpha_{B,pin1}$	1.39	1.00	0.81	1.11
$\alpha_{B,pin2}$	2.22	1.94	1.97	1.64

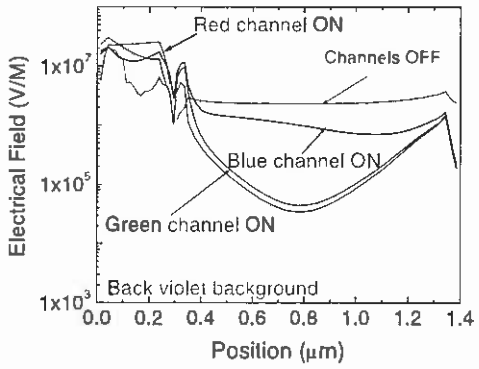

Fig. 7 Simulated electric field profile under back violet background without (OFF) or with the red, the green and the blue channels ON (ON)

the electric field there, and so, the red collection (Red ON) almost disappears ($\alpha_{R,pin2}{}^{V}<<1$). Blue channel is absorbed across the front diode where the electric field was enhanced resulting in an increase collection of the blue channel ($\alpha_{B,pin2}{}^{V}>1$). Since the green channel is absorbed across front and back diodes, its collection is balanced by the increase collection in the front diode and its reduction at the back ($\alpha_{G,pin2}{}^{V}\sim 1$). The front violet background is absorbed at the surface of the front diode, increasing the electric field at the back diode, where the red and part of the green channels generate optical carriers. So, the collection is strongly enhanced ($\alpha_{R,pin1}{}^{V}>>1$, $\alpha_{G,pin1}{}^{V}>1$) while the blue collection stays near its dark value ($\alpha_{B,pin1}{}^{V}\sim 1$).

Violet Optical Bias Control

Polychromatic combinations of the same red, green, and blue input channels of Fig. 6 but in different bit sequences were used to generate a multiplexed (MUX) signal. In Fig. 8, the filtered signals under front (pin_1) and back (pin_2) violet light control are displayed. The signals were normalized to the maximum intensity under violet front irradiations to suppress the dependence on sensor and LEDs positioning. The bit sequences used to transmit the information are shown at the top of the figures.

Different gains for the RGB channels were obtained (Table 1). Due to this wavelength nonlinearity under front violet background, the encoded multiplexed signal presents as many levels as the possible RGB combinations, in a maximum of 2^3 (eight-level encode). Those levels can be grouped into two main classes due to the high amplification of the red channel ($\alpha_{R,pin1}{}^{V}>>1$). The upper levels are ascribed to the presence of the red channel, and the lower to its absence allowing the red channel decoder. Since under front irradiation, the green channel is amplified ($\alpha_{G,pin1}{}^{V}>1$); the highest levels, in both classes, are ascribed to the presence of the green channel and the lower ones to its lack (long-pass filter). Under back irradiation, the red channel is suppressed ($\alpha_{R,pin2}{}^{V}<<1$), the blue enhanced ($\alpha_{B,pin2}{}^{V}>1$), and the green reduced ($\alpha_{G,pin2}{}^{V}<1$), so the encoded multiplexed signal presents a maximum of four separate levels (2^2). The highest levels correspond to the presence of the blue channel ON with or without the green ON, respectively, and the other to its absence. The blue channel is then decoded using this simple algorithm (short-pass filter).

Encoder/Decoder Device

A decoding algorithm was implemented in *Matlab* and tested. In order to make the decoding algorithm less dependent on sensor and LEDs positioning, the pin_1 and pin_2 signals were normalized to the maximum intensity of the pin_1 signal. In the second step, the intensity levels were determined by sampling and averaging in each time slot to minimize the effect of noise and interference from previous and subsequent time slots. At each time slot, a two-dimensional vector was defined having as one of the coordinates the sum of the intensity levels of pin_1 and pin_2 and their difference as the other coordinate. The rational for the choice of such basis set is that one of the coordinates weighs the number of channels that are "on" and the other weighs the red versus blue content of the measured signal.

This approach allows a clear separation of all RGB vectors in the two-dimensional space. The channels are then decoded using a simple Euclidean metric with precalculated vectors of all RGB combinations. The decoding is completed when the RGB combination of the closest precalculated vector is assigned to each time slot. In all tested sequences, the RGB signals were correctly decoded, as exemplified in Fig. 9. Here, on the top, the DEMUX signals obtained using the decoder algorithm are displayed. The correspondent binary bit sequences are in agreement with the optical signal used to transmit the information (Fig. 8).

Results show that by means of violet optical bias control, the MUX photonic function may be modified, giving reconfiguration. This new method, based on wavelength background processing techniques, enables the optical routing.

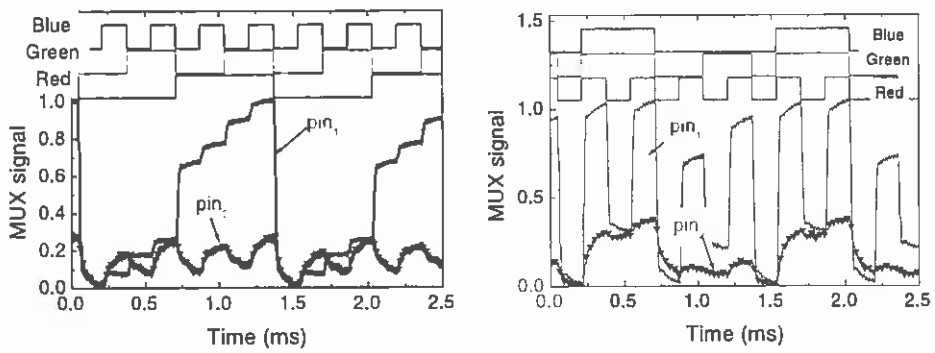

Fig. 8 Filtered output signals: a front (pin_1; *lines*) and back (pin_2; *symbols*) violet irradiation. On the *top*, the optical signal used to transmit the information guide the eyes

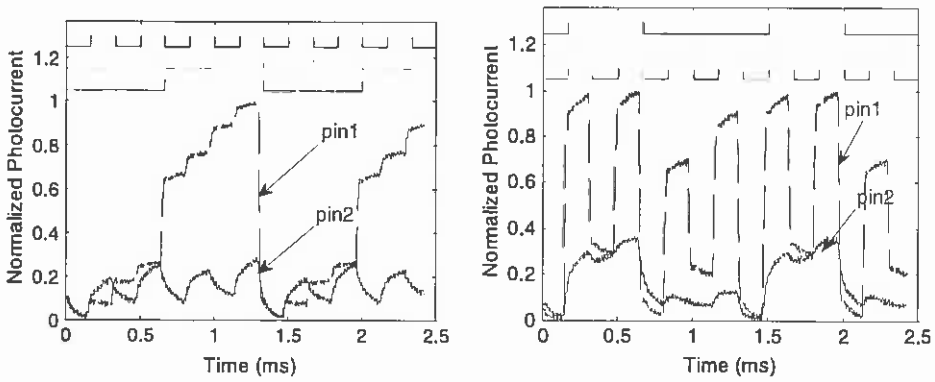

Fig. 9 MUX/DEMUX signals under front (*pin1*) and back (*pin2*) irradiation

Optoelectronic Model

Based on the experimental results and device configuration, an optoelectronic model supported by the complete dynamical large signal Ebers-Moll model with series resistors and capacitors was developed [7, 9]. The equivalent circuit, made out of a short-pass filter (front phototransistor, Q_1) and a long-pass filter (back phototransistor, Q_2) sections connected in parallel, is displayed in Fig. 10a.

The charge stored in the space charge layers is modeled by the capacitor C_1 and C_2. R_1 and R_2 model the dynamical resistances of the internal and back junctions under different dc bias conditions. To allow independent blue, red, and green channels transmission, four square wave current sources with different intensities are used: two of them, $\alpha_1 I_B$ and $\alpha_2 I_R$, with different frequencies to simulate the input blue and red channels and the other two, $\alpha_1 I_{Gpi\,n}$ and $\alpha_2 I_{Gpin}$, with the same frequency but different intensities, to simulate the green channel due to its asymmetrical absorption across both front and back phototransistors.

When the pi'npin device is reverse-biased, the base–emitter junction of both transistors are inversely polarized and conceived as phototransistors, taking, so, advantage of the amplifier action of adjacent collector junctions which are polarized directly. This results in a current gain proportional to the ratio between both collector currents. The amplifying elements, α_1 and α_2, can provide gain if needed and attenuate unwanted wavelengths (<1) while amplifying (>1) desired ones. The values and the strategic placement of the resistors determine the basic shape of the output signals. So, the flow of current through the resistor connecting the two transistor bases, R_1, is proportional to the difference in the voltages across both capacitors (charge storage buckets). The device is formed by two reconfigurable building blocks (the front and the back diodes) interconnected both optical and electrically, each of which has a distinct function. Depending on the side and wavelength of the optical bias control, the magnitude of the *signals* are changed by an α factor, and so the voltages across the front and the back or both photodiodes. The device behaves like an optoelectronic-controlled transmission system that stores, amplifies, and transports the minority carriers generated by the current pulses, through capacitors C_1 and C_2.

To validate the model under front and back violet irradiation, in Fig. 10b, the experimental (solid lines) and the simulated (symbols) waveform under negative bias and front and back backgrounds is shown. The bit sequences to drive the channels are shown in the top of the figure to guide the eyes. To simulate the violet background, the current sources intensities that model the input channels (individual channels, Fig. 6) were multiplied by the on/off ratio between the input channels with and without optical

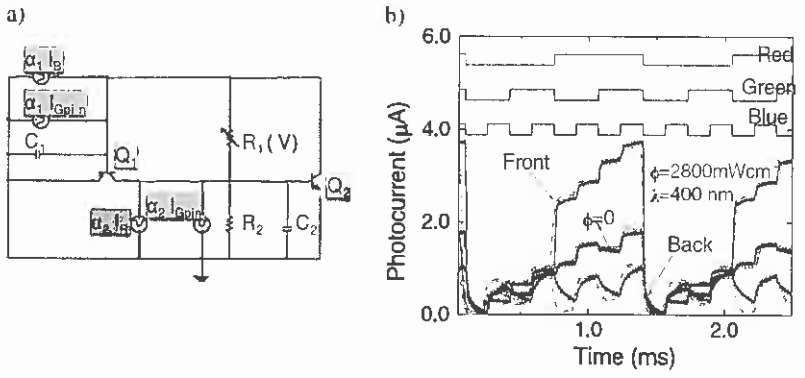

Fig. 10 **a** AC equivalent circuit. **b** Simulated (*symbols*) and experimental (*solid lines*) multiplex signals under front and back violet background

bias ($\alpha_{R,G,B\ pin1,2}$, V Table I). A good agreement between experimental and simulated data was achieved.

Under front irradiation, the expected optical amplification in the short wavelength range and quenching in the long ones is observed due to the effect of the active multiple-feedback filter when the back diode is light triggered. The opposite occurs under back irradiation.

Conclusions

WDM devices based on amorphous SiC multilayer filters were analyzed. Results show that the light-activated pi'n/pin a-SiC:H devices combine the demultiplexing operation with the simultaneous photodetection and self-amplification of an optical signal. The output waveform presents a nonlinear amplitude-dependent response to the wavelengths of the input channels. The background wavelength and irradiation side control the output signal. Depending on the wavelength of the external background and irradiation side, it acts either as a short- or a long-pass band filter or as a band-stop filter. MUX signals that perform 8-to-1 MUX function are compared. A decoding algorithm was implemented and tested. A two-stage active circuit is presented and gives insight into the physics of the device.

Acknowledgments This work was supported by FCT (CTS multi annual funding) through the PIDDAC Program funds and PTDC/EEA-ELC/111854/2009 and PTDC/EEA-ELC/120539/2010.

References

1. Iguchi Y, Yamabayashi N (2000) Proc 2th Int Conf InP and Related Mater 317:317–320
2. Bas M (2002) Chap. 13, McGraw-Hill, New York
3. Randel S, Koonen AMJ, Lee SCJ, Breyer F, Garcia Larrode M, Yang J, Ng'Oma A, Rijckenberg GJ, and Boom HPA (2007), ECOC 07 (Th 4.1.4), (pp. 1–4). Berlin, Germany
4. Vieira M, Louro, Fernandes M, Vieira MA, Fantoni A and Costa J (2011) Advances in Photodiodes, Gian Franco Dalla Betta (ed), ISBN: 978-953-307-163-3, InTech, Chap.19, pp: 403–425 (2011)
5. Louro P, Vieira M, Vieira MA, Fernandes M. and Costa J (2011) Advances in photodiodes, Gian Franco Dalla Betta (Ed.), ISBN: 978-953-307-163-3, InTech, Chap.19, pp. 377–402
6. Vieira MA, Louro P, Vieira M, Fantoni A, Garção AS (2011) Sensors & Transducers Journal Vol. 10, Special Issue, February 2011, pp.96-120. ISSN 1726–5479
7. Vieira M, Fantoni A, Fernandes M, Louro P, Lavareda G, Carvalho CN (2009) J Nanosci Nanotechnol 9(7):4022–4027
8. Ferlauto AS, Ferreira GM, Pearce JM, Wronski CR, Collins RW, Deng X, Ganguly G (2004) Thin Solid Films 455–456:388
9. Vieira MA, Vieira M, Fernandes M, Fantoni A, Louro P, Barata M (2009) Thin-film silicon science and technology. MRS Proc 1153, A08–A03